Fourier Transform Study of the Complex Electric Field Induced on Axially Heterostructured NWs

J. L. Pura, [1]* J. Jiménez [1]

1. GdS Optronlab, Dpt. Física de la Materia Condensada, Ed. LUCIA Universidad de Valladolid, Paseo de Belén 19, 47011 Valladolid, Spain

* Email: jlpura@fmc.uva.es

Abstract

We present in this work a study of the effect of Raman enhancement on axially heterostructured semiconductor nanowires (NWs). The investigation is motivated by the recent detection of a Raman signal enhancement effect at the heterojunction (HJ) of axially heterostructured NWs. Semiconductor NWs offer very interesting properties as compared to their bulk counterparts, making them the building blocks of future optoelectronic nanodevices. The use of HJs turns out to be essential for a great variety of devices. As a result, understanding the optical properties of heterostructured NWs is a fundamental step for their possible application on future technologies. In order to unveil the underlying physics of the light/NW interaction, the complex-valued electromagnetic (EM) field distribution induced inside heterostructured NWs under light exposure is studied. The use of the Fourier Transform is presented as a key tool in order to ascertain the different components of the EM field generated inside the NW. The results show the presence of two components: one associated with the incident light beam and a second one which appears as a consequence of the presence of the axial HJ. This second component explains the emergence of the Raman enhancement effect as a result of the interaction of the incident beam with the dielectric discontinuity associated with the HJ.

Keywords: nanowires, axial heterostructures, Fourier Transform, electromagnetic enhancement

1. Introduction

A great amount of research is being devoted to semiconductor nanowires (NWs) aiming to the fabrication of nanoscale devices. Semiconductor NWs present advantages with respect to thin films, as the possibility of combining highly mismatched materials, which allows for the growth of structures that are not available as thin layer devices [1, 2]. Furthermore, NWs were shown to be very efficient optical emitters and collectors [3], which makes them suitable for the development of high-performance photovoltaic cells [4], sensitive light detectors[5, 6], electro-optic modulators [7, 8], and light sources [9–11], among other applications. As mentioned above, NWs present large flexibility to be assembled in complex structures; in particular, a large range of mismatched heterostructures can be grown free of defects, as compared to the limitations imposed to thin films by large lattice mismatches. As a prerequisite for the extended use of these heterostructured NWs in photonic devices, one needs to understand the way in which they interact with light.

Geometrical optics applies to large objects, in this situation the absorption/scattering cross section is directly related with the geometrical cross section of the material, which results in absorption/scattering efficiencies between 0 and 1. However, when dealing with objects of subwavelength size the absorption/scattering efficiencies can scale to values well above unity [12, 13]. As a consequence of the subwavelength dimension and the large dielectric mismatch between the NW and its environment the effective light collection area is larger than the geometrical section of the object, i.e. the NW behaves as an optical nanoantenna. Furthermore, the electromagnetic resonances reported for semiconductor NWs can enhance the electromagnetic field by orders of magnitude, which points to the great potential of semiconductor NWs for photonic applications.

Most of the research about the optical properties of NWs concerns homogeneous NWs. In this case, Mie theory applies to the light scattering by NWs under illumination perpendicular to its axis; meanwhile, vertically aligned NWs illuminated parallel to its axis can support guided modes, even conforming Fabry-Perot cavities [14].

Complex structures based on heterojunctions (HJ) must be included in a great number of devices. Understanding the role of these HJs is a crucial issue for their use in advanced photonic devices. Carefully controlling the HJ properties during growth [15] is equally important as studying the properties of the HJs under light illumination. In bulk materials, light/semiconductor interaction is solely governed by the refractive index; however, subwavelength diameter semiconductor NWs exhibit resonances related to other factors like their size, shape and composition [16, 17]. On the other hand, the scattering cross section of these systems strongly depends on the NW orientation

with respect to the light polarization, another sign of the drastic difference between the NWs behaviour and their bulk counterpart.

Luminescence emitters have been previously used to study this phenomenon. However, the spontaneous radiative emission in semiconductor NWs is sometimes suppressed by the surface recombination. Furthermore, luminescence emission, if any, is weak in the case of Si and SiGe NWs, all these factors make it difficult to quantify the changes in the spontaneous emission [18]. Unlike luminescence emission, Raman scattering is less sensitive to the surface state, moreover, it can be observed for any semiconductor and excitation wavelength, independently of their radiative recombination efficiency. Thus, Raman scattering can be used as an alternative way to study the interaction between light and complex heterostructured semiconductor NWs. For Raman scattering, the signal intensity is proportional to the electromagnetic field intensity, i.e. $|E|^2$, which allows studying the distribution of the radiation inside heterostructured systems.

The diameter dependence of the light scattering resonances can be explained in the Mie scattering framework, where the eigenfunctions of the Mie solution of Maxwell equations are coupled with the NW diameter, giving the Mie resonances [19, 20]. Usually, this approach is applied to infinite homogeneous NWs. Alternatively, finite element methods (FEM) can be used to solve the Maxwell equations of the system formed by the light and the finite NW. A significant body of research has been devoted to homogeneous infinitely long NWs, while, a detailed analysis of the interaction of light with finite length NWs and heterostructured NWs is still lacking.

Recently, we have reported a significant local enhancement of the Raman signal at the heterojunction of axially heterostructured Si/SiGe NWs [21, 22] and Si/InAs NWs [23]. This is an interesting issue since the enhancement of the electromagnetic field at the HJ of NWs should provide an additional degree of freedom to engineer the photon absorption and scattering by semiconductor NWs, which should permit to operate photons over different optical resonances. Nevertheless, further research effort is needed to understand this interaction.

We present herein an analysis of the semiconductor NW/ light interaction based in the numerical solution of the Maxwell equations by FEM of group IV NWs, in particular, homogeneous Si NWs and axially heterostructured Si/SiGe NWs. This study entails both plane wave illumination and illumination with a focused laser beam allowing to reproduce the conditions of micro-Raman and micro-PL experiments.

2. Finite Element Method Model and Results

The FEM simulations were performed by using the Electromagnetic Waves in Frequency Domain module of COMSOL Multiphysics. The air/NW/substrate system is simulated using the same arrangement of the experimental measurements, i.e. the NWs are lying flat over an Al substrate, and the dimensions of the NWs (diameter, length, etc) were selected to match those of the typically investigated NWs. Further details about the FEM model can be found elsewhere [21, 22].

By using this model, a full 3D solution of the Maxwell equations was performed in order to ascertain the effect of the NW length and the presence of the axial HJs over the light/NW interaction. The first simulation concerns the study of the simplest case: a Si NW of varying length under plane wave excitation ($\lambda = 532$ nm). The calculated value of $|E|^2$ is plotted for different NW lengths in Figure 1a. In particular, for plane wave illumination of a homogeneous NW, longitudinal modes are observed, contrarily to an infinite NW that did not exhibit any longitudinal modes. After this, a SiGe/Si axially heterostructured NW under plane wave illumination was studied, Figure 1b. The pattern is very similar to the homogeneous NW, but the EM field enhancement at the HJ can be observed. Furthermore, the coupling of the incident plane wave with the material change of the HJ modifies the longitudinal modes of the EM field distribution on its vicinity.

The first simulation of a homogeneous Si NW was repeated for local illumination using a focused Gaussian beam, Figure 1c. These illumination conditions are much closer to the real experiments of μ-Raman and μ-photoluminescence. In this situation, the longitudinal modes only appear when the NW end is illuminated by the laser beam. These modes are not observed for homogeneous NWs and local illumination at the central region of the NW when the laser beam does not reach the NW ends. According to the infinite extension of a plane wave longitudinal modes always appear for plane wave illumination. Note that these longitudinal modes cannot be associated with guided modes since the incident wave arrives perpendicular to the NW axis (TM polarization with respect to the NW axis) which is not suitable for the transmission of light along the NW. Moreover, the SiGe absorption coefficient for 532 nm light is relatively large, especially when increasing the Ge content, which gives a very short light path inside the NW (the values range from ≈ 18 nm for pure Ge, to ≈ 890 nm for pure Si). Similar behaviour was reported in [24], where second harmonic generation (SHG) oscillations were observed when the light source illuminate the NW ends, but the SHG oscillations were absent when the light source hits the NW body without affecting the NW ends. SHG modes are sustained by the distribution of the internal optical field [25].
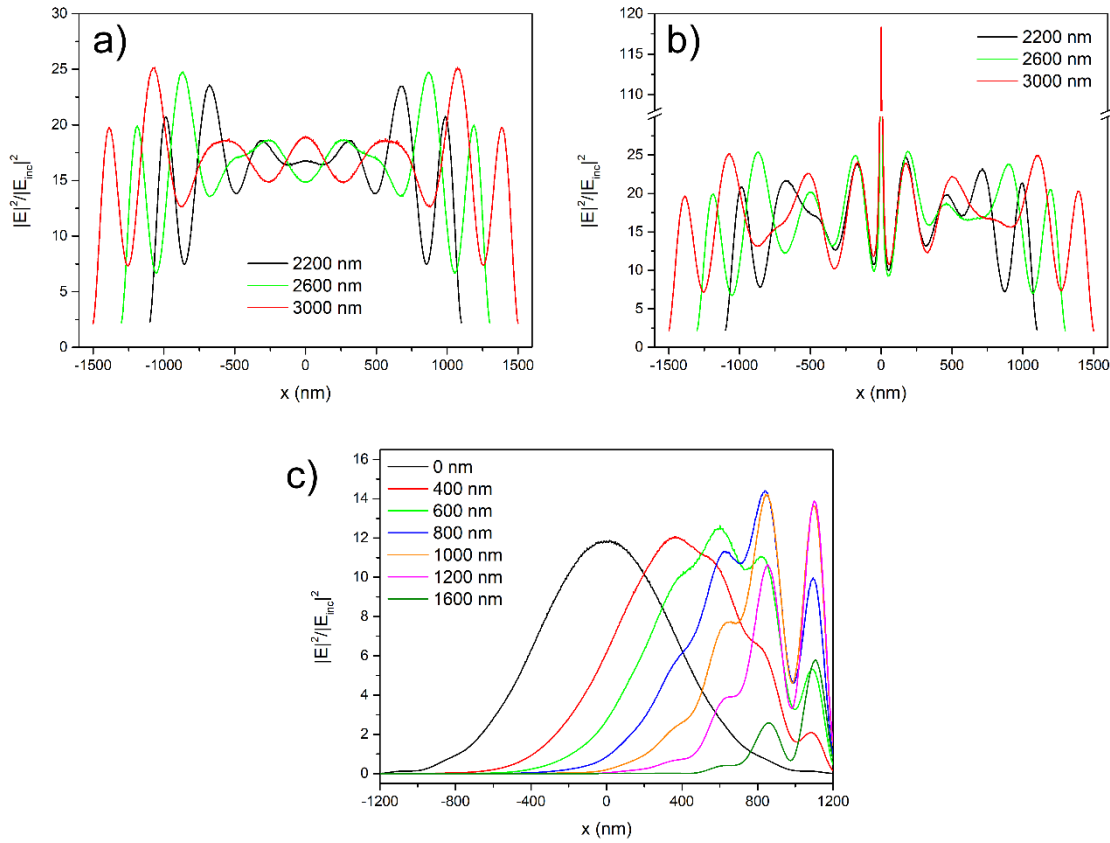
Figure 1. *a) EM field distribution inside a homogeneous Si NW for different NW lengths and plane wave illumination. b) EM field distribution inside a SiGe/Si axially heterostructured NW for different NW lengths and plane wave illumination. c) EM field distribution inside a homogeneous Si NW under Gaussian beam illumination for different positions of the beam focus.*

Upon the above observations, one can say that the longitudinal modes are due to the disturbance of the electromagnetic field by the end boundaries of the NW. One cannot define an effective wavelength for the longitudinal modes for long NWs just by visual inspection of the EM field. In fact, the separation between the successive maxima depends on the NW length and on the distance to the NW ends. These oscillations are determined by the boundary conditions at the NW ends and are sustained by the incident electromagnetic wave. Therefore, the electromagnetic field inside the NW is modulated by the field coupling with the NW boundaries. An analogous effect occurs when the light beam hits the HJ.

3. Fourier Transform study of the Electric Field

In order to better understand the role of the HJ and its effect on the electromagnetic field, we performed a Fourier Transform study of the electromagnetic field distributions inside the NW. For this purpose, a standard Fast Fourier Transform (FFT) [26] is applied to the complex-valued electric field distribution to obtain its principal Fourier components. Figure 2 shows the electric field distribution of two different NWs used as an example. Both are 1 μm long, one is a homogeneous Si NW and the other one a heterostructured Si/SiGe NW. It can be observed that the presence of the HJ, located at the NW centre, disturbs the field distribution raising its value around this position, which explains the already mentioned enhancement effect.

FFT was applied over this EM field distributions (note that the FFT operation is performed over the complex valued original data and not the field modulus). The results are shown in Figure 3.
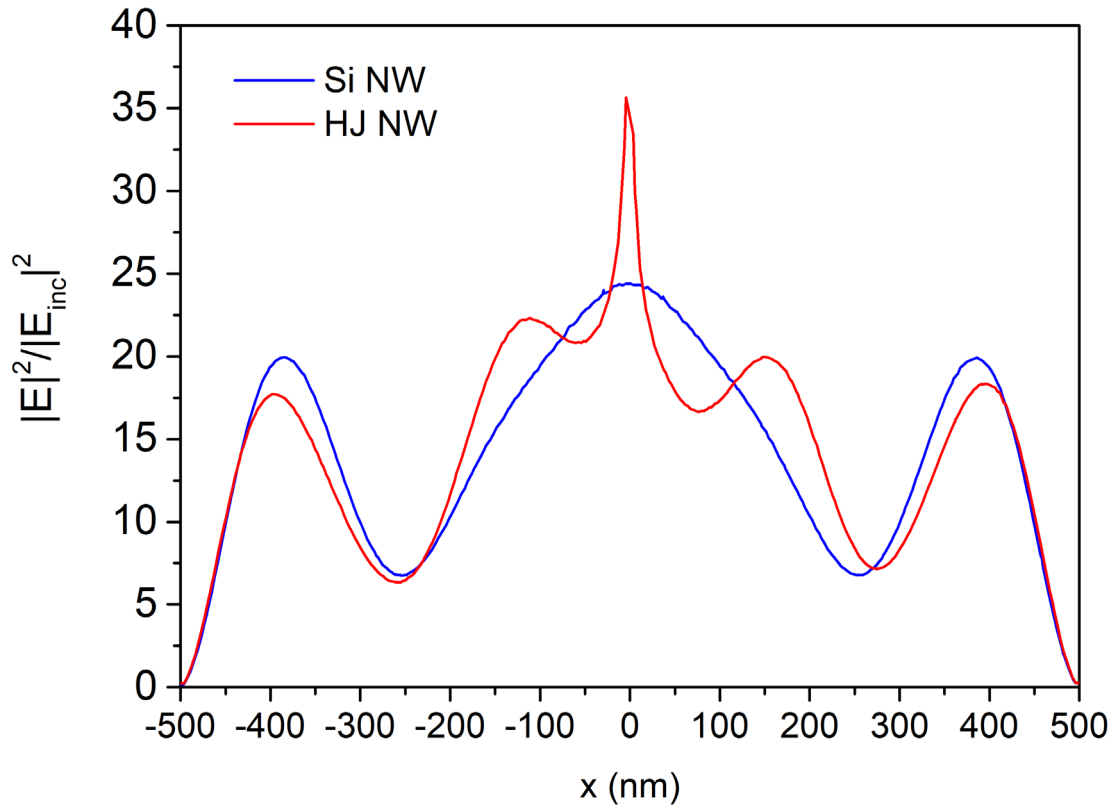

Figure 2. *Distribution of the electric field modulus along the axis of a 1 μm Si NW and a 1 μm Si/SiGe heterostructured NW under 532 nm plane wave illumination.*
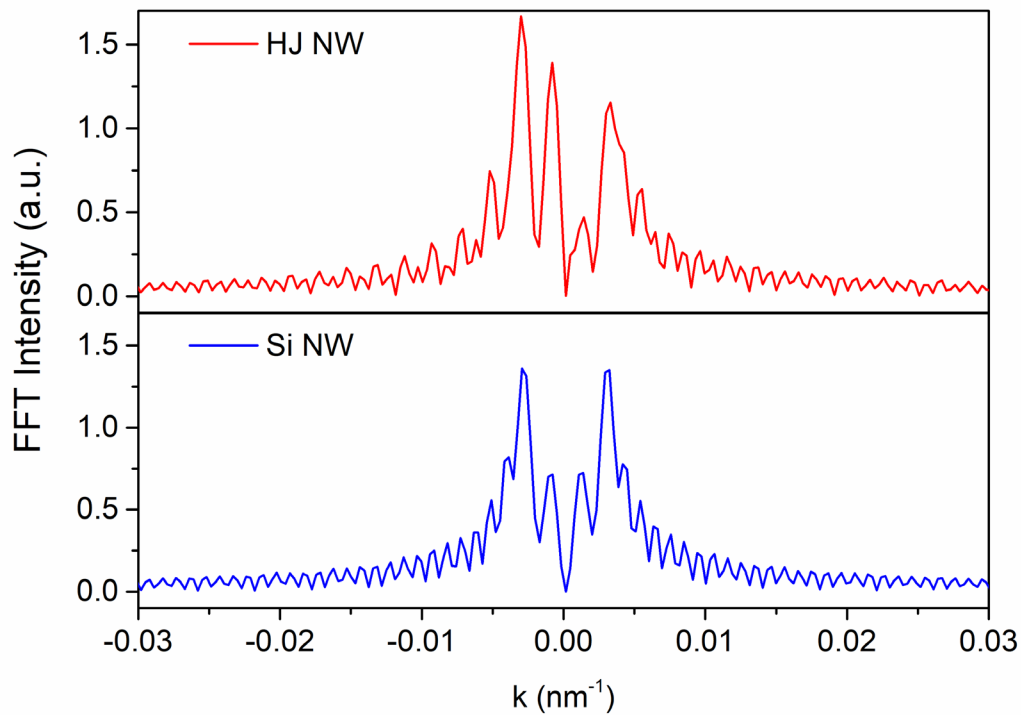
Figure 3. *Fast Fourier Transform intensities obtained from the electric field profiles of Fig. 2. There are 2 symmetric peaks on the Si NW that remain visible in the heterostructured NW. However, the SiGe/Si NW presents a new asymmetric structure that results in a new peak on the negative side, and symmetrically lowers the FFT on the positive side. The symmetric peak can be associated with the principal component of the field, 532 nm light, while the antisymmetric one is induced by the presence of the HJ.*

The Fourier Transform of the Si NW shows the main component of the field which is symmetric in k-space. However, if we look at the FFT of the HJ NW the plot is completely different. We can see that the main shape is similar to the Si NW FFT but it is no longer symmetric. If the plot is carefully analysed we could detect that the negative symmetric peak is increased, while the positive symmetric peak is decreased. Therefore, there is a new contribution which appears at symmetric values of k, but with opposite signs, i.e. an antisymmetric component, see Figure 4.
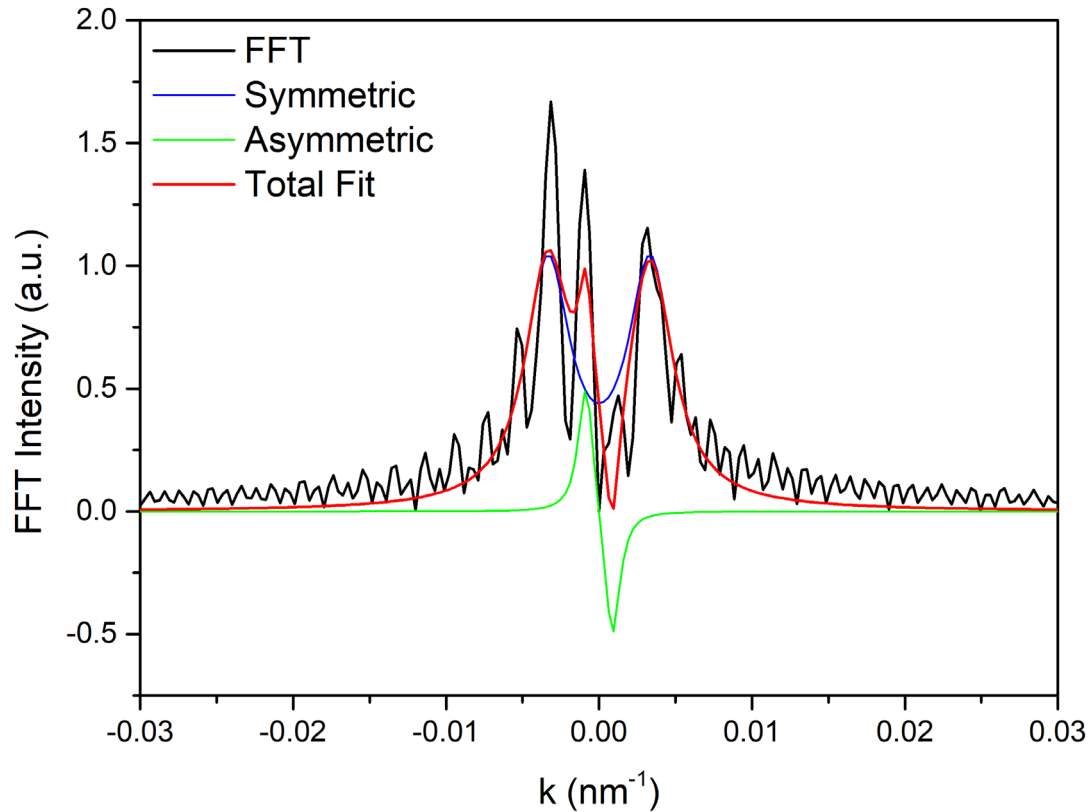
Figure 4. *Example of the fit of the FFT data by using two components: symmetric (blue curve) and antisymmetric (green curve).*

In order to ascertain the origin of these two components we performed an analysis of their dependence with the NW length and the incident light wavelength. The results are summarized in Figure 5.

The position of the symmetric component turns out to be independent of the NW length and only varies with the incident light wavelength, Figure 5a. This direct correlation with the incident light wavelength tells us that this component is precisely the main component of the field. Conversely, the antisymmetric peak position changes with the NW length but it is independent of the incident wavelength, Figure 5b. We can conclude from this information that the presence of the HJ is adding a contribution to the EM field that modifies its distribution and is directly related to the discontinuity along the NW axis, according to its dependence on the NW length. It is worth noting that for high values of the incident wavelength (600 nm on Figure 4a) there is a subtle dependence of the symmetric peak position with the NW length, which is followed by the predicted independence for higher values. This is an expected behaviour since a wavelength of 600 nm is comparable to the first two values of NW length that have been simulated, and for these values the interaction with the NW length modifies the fundamental mode wavelength.
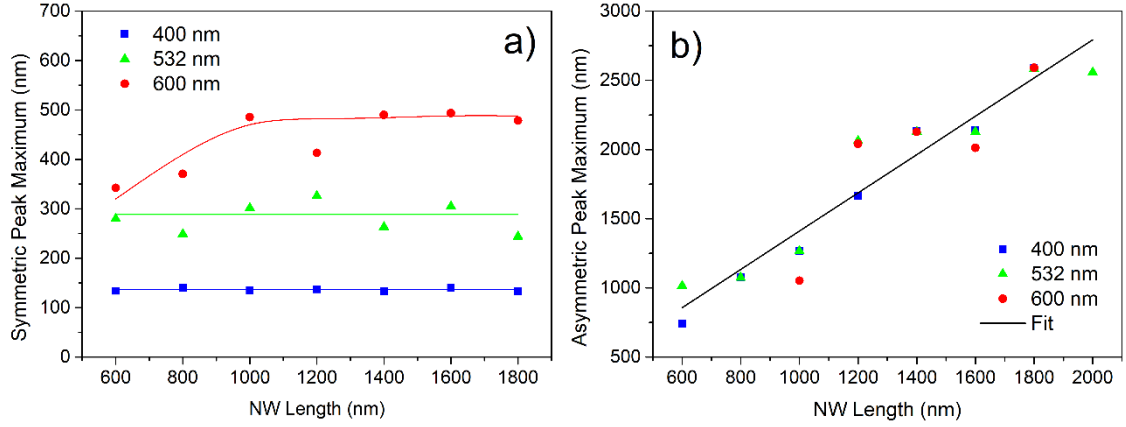
Figure 5. *a) Position on k-space of the symmetric peak as a function of the NW length for different incident wavelengths, showing its dependence on the light wavelength and independence on NW length. b) The same plot for the antisymmetric peak, showing the opposite behaviour, linear dependence with NW length and independence on the incident light wavelength.*

According to this, the symmetric mode would correspond to the natural mode of the 532 nm light inside the NW. The even symmetry of this peak in Fourier space will result in the electric field having a large real part, as a consequence of Fourier Transform properties. On the other hand, the antisymmetric peak will represent the effect of the HJ inducing a stationary wave, and its odd symmetry results in a large imaginary part ($\pi/2$ phase shift) on the electric field. Essentially, symmetric functions result in real valued functions under inverse Fourier transform (e.g. cosine function), while antisymmetric functions result in pure imaginary functions (e.g. sine function).

If we come back to Figure 3, the relation between the k value of the main symmetric component (propagation constant), and the corresponding value of the wave vector in vacuum, $k_0 = 2\pi/\lambda_0$, allow us to calculate the effective refractive index (or mode index)

$$n_{eff} = \frac{k}{k_0}$$

As we have already mentioned this effective index depends exclusively on the incident wavelength, and not on the NW length. Figure 6 shows the dependence of the effective index with the incident wavelength.
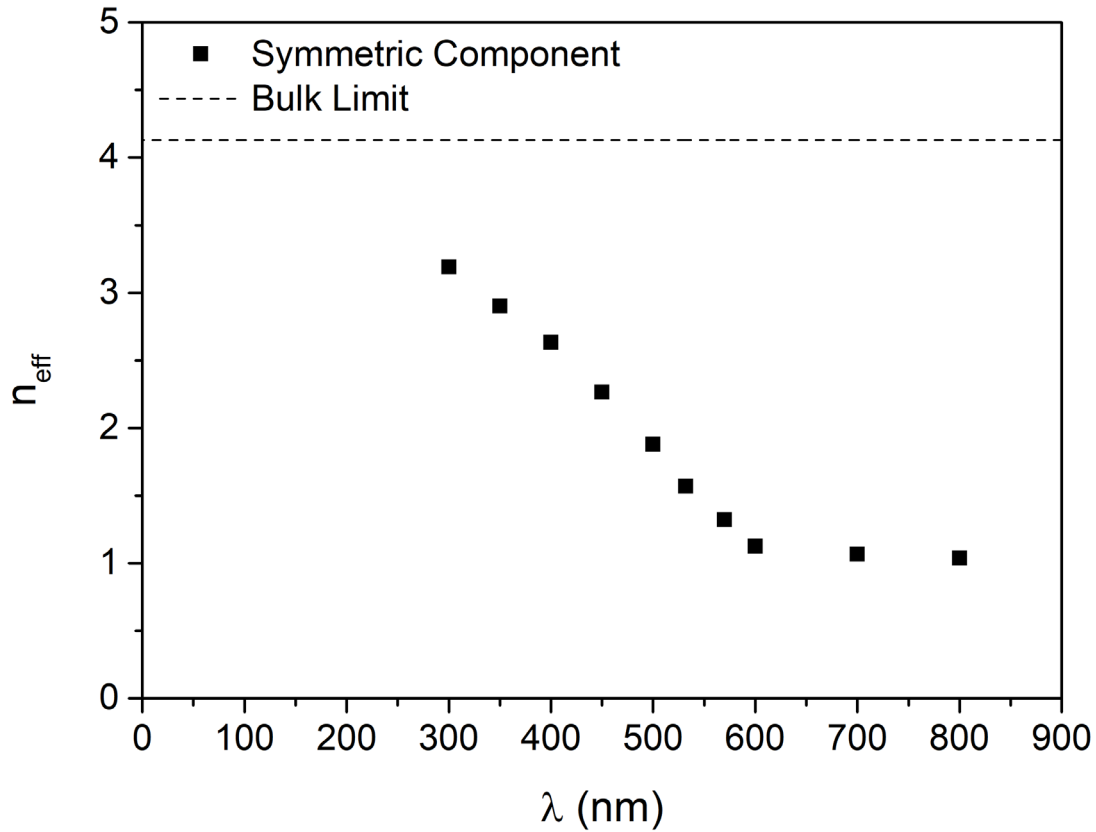
Figure 6. *Dependence of the effective index with the incident wavelength for a 45 nm diameter NW. There are two limiting regions: for λ << d the wave "sees" the NW as infinite, and the refractive index tends to be that of bulk Si (~ 4.13); for λ >> d the NW is too small to be "seen" by the incident wave and it behaves as if it were transparent, the index tends to be that of air.*

In Figure 6 we can see two different physical limits:

- for $\lambda \ll d$ the incident wave interacts with the NW as if it was infinite (bulk), and the refractive index tends to be that of bulk Si (~ 4.13).

- for $\lambda \gg d$ the NW is too small to interact with the incident wave and it behaves as if it was transparent, the index tends to be that of air.

It is important to note that this effective index is not a proper refractive index, i.e. it does not involve a travelling wave. This number just evidences the supported wavelength inside the NW. It can be understood as the degree of interaction between the NW and the incident electromagnetic field [24, 27].

Conclusions

The effect of the HJ of axially heterostructured NWs on the EM field distribution under light illumination has been investigated. The results show a clear coupling between the incident EM field and dielectric discontinuity of the axially heterostructured NW, which results in the enhancement of the EM field around this region. The Fourier analysis reveals the existence of a new field component on heterostructured NWs, as compared with homogeneous NWs. This mode is antisymmetric in k-space, contrary to the principal mode of the incident light which is symmetric. The study of the dependence of these two modes with both the incident light wavelength and the NW length accounts for their respective origins. The symmetric peak varies with the incident light wavelength and it is independent on the NW length, while the antisymmetric peak has the opposite behaviour, having a direct dependence with the NW length and being clearly independent of the incident light wavelength. Finally, the effective index of the symmetric mode is studied, showing a dependence of the light/NW interaction as a function of the incident wavelength. For large values of the wavelength it can be observed that the light does not interact with the NW, because it is much smaller than one wave cycle. For small values of the wavelength the NW behaves bulk-like, showing the response of an ordinary travelling wave. It is in the intermediate region (the visible range) in which the light strongly interacts with the NW, changing the effective refractive index. These results shed light on the phenomenon of light/NW interaction, particularly in the case of axially heterostructured ones, for their application on future optoelectronic nanodevices, like light sensors or solar cells, among others.

Acknowledgements

References

[1]   M. J. Tambe; S. K. Lim; M. J. Smith; L. F. Allard; and S. Gradečak, Realization of defect-free epitaxial core-shell GaAs/AlGaAs nanowire heterostructures, *Appl. Phys. Lett.*, **93**, 15, 2013–2016.

[2]   U. Krishnamachari; M. Borgstrom; B. J. Ohlsson; N. Panev; L. Samuelson; W. Seifert; M. W. Larsson; and L. R. Wallenberg, Defect-free InP nanowires grown in [001] direction on InP (001), *Appl. Phys. Lett.*, **85**, 11, 2077–2079.

[3]   S. K. Saini and R. V. Nair, Quantitative analysis of gradient effective refractive index in silicon nanowires for broadband light trapping and anti-reflective properties, *J. Appl. Phys.*, **125**, 10.

[4]   J. Wallentin *et al.*, InP Nanowire Array Solar Cells Achieving 13.8% Efficiency by Exceeding the Ray Optics Limit, *Science (80-.).*, **339**, 6123, 1057–1060.

[5]   Y. H. Ahn and J. Park, Efficient visible light detection using individual germanium nanowire field effect transistors, *Appl. Phys. Lett.*, **91**, 16, 8–11.

[6]   C. Soci; A. Zhang; B. Xiang; S. A. Dayeh; D. P. R. Aplin; J. Park; X. Y. Bao; Y. H. Lo; and D. Wang, ZnO Nanowire UV Photodetectors with High Internal Gain, *Nano Lett.*, **7**, 4, 1003–1009.

[7]   A. B. Greytak; C. J. Barrelet; Y. Li; and C. M. Lieber, Semiconductor nanowire laser and nanowire waveguide electro-optic modulators, *Appl. Phys. Lett.*, **87**, 15, 1–3.

[8]   B. Piccione; C. H. Cho; L. K. Van Vugt; and R. Agarwal, All-optical active switching in individual semiconductor nanowires, *Nat. Nanotechnol.*, **7**, 10, 640–645.

[9]   J. Bao; M. A. Zimmler; F. Capasso; X. Wang; and Z. F. Ren, Broadband ZnO Single-Nanowire Light-Emitting Diode, *Nano Lett.*, **6**, 8, 1719–1722.

[10]   C. P. T. Svensson; T. Mårtensson; J. Trägårdh; C. Larsson; M. Rask; D. Hessman; L. Samuelson; and J. Ohlsson, Monolithic GaAs/InGaP nanowire light emitting diodes on silicon, *Nanotechnology*, **19**, 30, 305201.

[11]   C. P. T. Svensson; W. Seifert; M. W. Larsson; L. R. Wallenberg; J. Stangl; G. Bauer; and L. Samuelson, Epitaxially grown GaP/GaAs $_{1-x}$ P $_x$ / GaP double heterostructure nanowires for optical applications, *Nanotechnology*, **16**, 6, 936–939.

[12]   D. V Murphy and S. R. J. Brueck, Enhanced Raman scattering from silicon microstructures, *Opt. Lett.*, **8**, 9, 494.

[13]   G.-H. Ding; C. T. Chan; Z. Q. Zhang; and P. Sheng, Resonance-enhanced optical annealing of silicon nanowires, *Phys. Rev. B*, **71**, 20, 205302.

[14]   X. Duan; Y. Huang; R. Agarwal; and C. M. Lieber, Single-nanowire electrically driven lasers, *Nature*, **421**, 6920, 241–245.

[15]   J. L. Pura; P. Periwal; T. Baron; and J. Jiménez, Growth dynamics of SiGe nanowires by the vapour-liquid-solid method and its impact on SiGe/Si axial heterojunction abruptness, *Nanotechnology*, **29**, 35, 355602 (9pp).

[16]   M. Khorasaninejad; S. Patchett; J. Sun; N. O; and S. S. Saini, Diameter dependence of polarization resolved reflectance from vertical silicon nanowire arrays: Evidence of tunable absorption, *J. Appl. Phys.*, **114**, 2, 024304.

[17]   F. J. Lopez; J. K. Hyun; U. Givan; I. S. Kim; A. L. Holsteen; and L. J. Lauhon, Diameter and polarization-dependent raman scattering intensities of semiconductor nanowires, *Nano Lett.*, **12**, 5, 2266–2271.

[18]   G. Bourdon; I. Robert; R. Adams; K. Nelep; I. Sagnes; J. M. Moison; and I. Abram, Room temperature enhancement and inhibition of spontaneous emission in semiconductor microcavities, *Appl. Phys. Lett.*, **77**, 9, 1345–1347.

[19]   G. Brönstrup *et al.*, A precise optical determination of nanoscale diameters of semiconductor nanowires., *Nanotechnology*, **22**, 385201.

[20]   L. Cao; P. Fan; A. P. Vasudev; J. S. White; Z. Yu; W. Cai; J. A. Schuller; S. Fan; and M. L. Brongersma, Semiconductor nanowire optical antenna solar absorbers, *Nano Lett.*, **10**, 2, 439–445.

[21]   J. L. Pura; J. Anaya; J. Souto; Á. C. Prieto; A. Rodríguez; T. Rodríguez; and J. Jiménez, Local electric field enhancement at the heterojunction of Si/SiGe axially heterostructured nanowires under laser illumination, *Nanotechnology*, **27**, 45, 455709.

[22]   J. L. Pura; J. Anaya; J. Souto; A. C. Prieto; A. Rodríguez; T. Rodríguez; P. Periwal; T. Baron; and J. Jiménez, Electromagnetic field enhancement effects in group IV semiconductor nanowires. A Raman spectroscopy approach, *J. Appl. Phys.*, **123**, 11, 114302.

[23]   J. L. Pura; A. J. Magdaleno; D. Muñoz-Segovia; M. Glaser; A. Lugstein; and J. Jiménez, Electromagnetic enhancement effect on the atomically abrupt heterojunction of Si/InAs heterostructured nanowires, *J. Appl. Phys.*, **125**, 6, 064303.

[24]   R. Grange *et al.*, Far-field imaging for direct visualization of light interferences in GaAs nanowires, *Nano Lett.*, **12**, 10, 5412–5417.

[25]   R. Cisek; V. Barzda; H. E. Ruda; and A. Shik, Nonlinear Optical Properties of Semiconductor Nanowires, *IEEE J. Sel. Top. Quantum Electron.*, **17**, 4, 915–921.

[26]   R. Bracewell, *The Fourier Transform and Its Applications*, 3rd ed.; McGraw-Hill, 1963.

[27]   L. Tong; J. Lou; and E. Mazur, Single-mode guiding properties of subwavelength-diameter silica and silicon wire waveguides., *Opt. Express*, **12**, 6, 1025–1035.